Ionosphere Sounding in the Central Arctic: Preliminary Results of the Multidisciplinary Drifting Observatory for the Study of Arctic Climate (MOSAiC) Expedition

Maximilian Semmling, Jens Berdermann, Martin Kriegel, Friederike Fohlmeister, and Hiroatsu Sato

Abstract – We report on an experiment conducted during the expedition of the Multidisciplinary Drifting Observatory for the Study of Arctic Climate (MOSAiC) in 2019 and 2020. Signals of global navigation satellite systems (GNSS) were recorded during 12 months aboard the German research icebreaker Polarstern that drifted with a sea ice floe over the Arctic Ocean. Here, we focus on an ionosphere sounding experiment and present preliminary results from a 5 month period in the central Arctic (>85° N). Based on the standard deviations of phase samples (phase scintillation index), we found ship-related disturbances and anomalies, indicating space weather impact on GNSS signals. The ship-related disturbances with values up to 0.4 rad, attributed to mast and chimney shadowing, are masked out. Anomalies can be resolved with index values of 0.15 rad to 0.2 rad that are attributed to variations of ionospheric electron density in the cusp region. The baseline of GPS index observations with this shipborne setup lies at ≈0.1 rad for elevations >30° and reaches up to 0.17 rad at lowest elevations. This baseline for the drifting ship is significantly higher than the baseline of up to 0.05 rad found for ground-based stations equipped with the same receiver type. We conclude that ionospheric phase scintillation in GNSS signals can be detected from a ship drifting with the Arctic ice. Restrictions due to shadowing and increased noise level of the ship scenario have to be considered.

1. Introduction

The Arctic is still a challenging destination for geophysical monitoring. The absence of islands in the central Arctic (>85° N) causes a lack of ground-based stations for monitoring. Research vessels can add important observations to monitor the Arctic. The monitoring task is important as navigation and activities in several economic sectors (e.g., oil, gas and mineral industries, fishery, forestry, and tourism) will increase in the Arctic with global warming and the reduction of sea ice cover. Space weather poses an important monitoring task with the potential effect on the mentioned activities that need accurate and continuous services for navigation, communication, and environmental monitoring. The signals of satellite-based communication, navigation, and remote sensing systems are subject to interaction with ionospheric plasma. Space weather can cause disturbances in the ionosphere that lead to changes in amplitude, phase, polarization, and delay of radio signals. These ionospheric irregularities manifest themselves in technical applications as measurement errors or even signal loss. The polar regions are strongly driven by continuous and spontaneous space weather conditions due to the topology of the Earth geomagnetic field. The dynamics with high local and spatial variability in high latitudes are not completely understood so far but lead to a frequent impact on technologies and to economic loss. We investigate the space weather impact on global navigation satellite system (GNSS) data recorded on a ship in the central Arctic. The study is linked to the expedition of the German research icebreaker Polarstern, [1] as part of Multidisciplinary Drifting Observatory for the Study of Arctic Climate (MOSAiC) [2], and is part in a series of studies focusing on GNSS for remote sensing application within MOSAiC and previous scientific cruises to the Arctic: for atmospheric sounding [3, 4] and for sea ice characterization [5–7]. An ionospheric sounding approach is used to detect space weather-induced scintillations as described by [8]. The data were recorded on Polarstern during MOSAiC in 2019 and 2020. The focus lies on the phase scintillation index σ_ϕ.

Manuscript received 19 December 2022.

Maximilian Semmling, Jens Berdermann, Martin Kriegel, and Hiroatsu Sato are with the German Aerospace Center, Institute for Solar-Terrestrial Physics, Kalkhorstweg 53, 17235 Neustrelitz, Germany; e-mail: maximilian.semmling@dlr.de.

Friederike Fohlmeister is with the German Aerospace Center, Institute of Communication and Navigation, Münchener Strasse 20, 82234 Wessling, Germany.

2. Setup and Experiment

The GNSS scintillation measurement setup consists of a commercial receiver (Javad Delta) for continuous data recording (cf. [9]) and of a bitgrabber solution to record raw *L*-band samples of selected time periods. We concentrate here on observations of the Javad Delta receiver that provided continuous data of signal amplitude and phase with 50 Hz. The instrument was installed and operated on Polarstern in cooperation with the MOSAiC consortium, the Institute of Communications and Navigation, and the Institute for Solar-Terrestrial Physics. The receiver was equipped with a

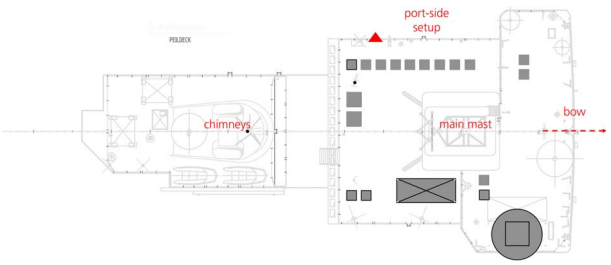

Figure 1. Map of observation deck on Polarstern with German Aerospace Center setup (red triangle) pointing portside to the sea (left from the indicated bow direction). Obstacles appear on the setup's backside toward the ship (main mast and chimneys).

multifrequency GNSS antenna (Javad Gr-Ant) that was mounted on the ship's observation deck; see portside setup in Figure 1.

Note that the main mast and the ship's chimney extend in height significantly (more than 5 m) above the observation deck. That leads to a shadowing of GNSS observation links in at least two directions seen from the setup (antenna) position (cf. respective items in Figure 1).

The observations have been recorded in an overall period from September 28, 2019, to October 10, 2020. We select a period of 5 mo (November 1, 2019, to March 31, 2020) when the ship was drifting with the ice floe in the central Arctic (above 85° N); see the trajectory on the map in Figure 2). For this drift period, the ship's heading plays an important role for the orientation of the receiving antenna relative to the transmitting satellite and for related changes in shadowing. The heading only very slowly changes during the 5 mo period. It is determined by the orientation of the ice floe to which the ship is attached to. By contrast, the course of the ship, when drifting with the floe, changes rather often (cf. respective plots in Figure 2).

The ship's heading very slowly changes from SW over S to E during the central Arctic period. Considering the portside location of the setup, we can expect best view to portside (that means 90° left of the ship's heading). The portside vector changes in the topocentric frame, according to the heading changes from SE over E to N. The topocentric azimuth angle of satellite links is converted to the respective relative bearing in the ship's body frame to better understand shadowing of ship structure (mast and chimney).

3. Preliminary Results and Discussion

The phase scintillation index σ_ϕ is derived from the 50 Hz receiver output by detrending the phase and computing the standard deviation of the residual over 60 s (cf. [10]). The scintillation index data are available via the PANGAEA server of Alfred Wegener Institute (AWI) https://doi.pangaea.de/10.1594/PANGAEA.956019 [11]. The detrending cuts off frequencies <0.1 Hz using a sixth order Butterworth filter. It is known that the index retrieved with this scheme can be

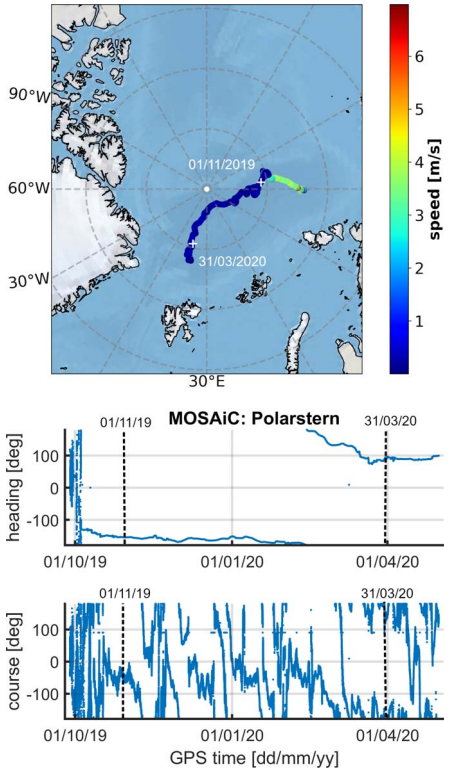

Figure 2. Trajectory of Polarstern during early drift during winter period (November 1, 2019, to March 31, 2020) in central Arctic (latitude >85°).

affected by diffractive and refractive contributions of the high-latitude ionosphere [12]. Differing between diffraction and refraction effects of the ionosphere is of minor importance in this study, as we concentrate on the separation of ionospheric effects from other impacts. The first results focus on variation of σ_ϕ with the relative bearing of the satellite on the ship to study the impact of shadowing. The relative bearing β is defined relative to the heading (0°), starting from backward (aft; –180°) over portside (–90°), forward bow (0°), and starboard (90°) to again backward (aft; 180°).

3.1 Inclination Effect and Ship-Related Disturbance

Figure 3 shows the two-dimensional (2D) histogram of σ_ϕ, dependent on β for different elevation ranges: high (>45°); medium (>30° and ≤45°); low (>10° and ≤30°); and lowest (≤10°). For high elevations, we find that the essential part of observations lies between portside, forward, and starboard ($-90° < \beta < 90°$), explained by the inclination of the GPS orbits. At high northern latitudes, due to the inclination, GPS satellites appear only in a southern direction at high elevations. In the given period, the ship's heading is mainly southward, which agrees with the observed bearing range. Furthermore, a significant disturbance with increased σ_ϕ occurs with $\beta \approx 45°$ (at high elevations and also below). This disturbance is

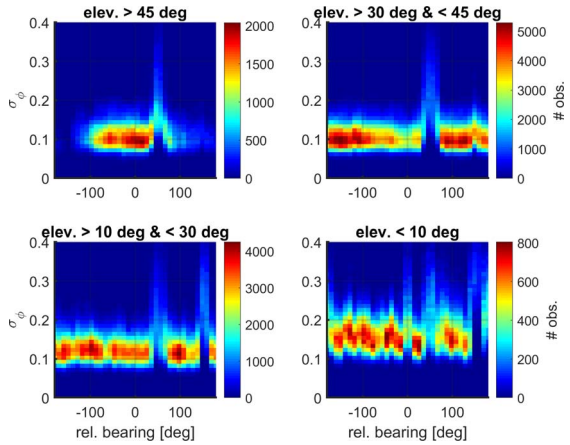

Figure 3. Distribution of σ_ϕ in radians over relative bearing from the setup on the ship. Four panels are shown with high, medium, low, and lowest elevations, respectively. Observations of the entire drift period (November 2019 to March 2020) are considered.

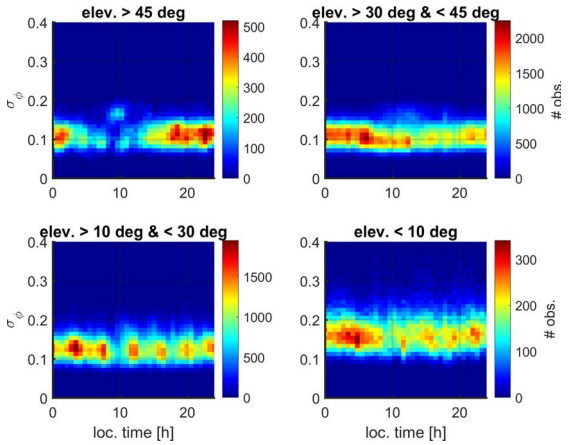

Figure 4. Distribution of σ_ϕ in radians over local time at IPP. Panels with high, medium, low, and lowest elevations are distinguished. At high elevations, an anomaly significantly increased σ_ϕ, occuring at about 10 h, which is most likely related to disturbance in the cusp region.

attributed to shadowing of the main mast that has the respective relative bearing seen from the portside setup (cf. Figure 1).

For medium elevations, the distribution peak is clearly shifted. A major part of observations lies backward and a minor part in a forward direction, which are also consequences of orbit inclination. Observations to the north are not found at high elevations; however, they accumulate at medium elevations. Again, there is a clear main mast disturbance ($\beta \approx 45°$). Another still minor disturbance occurs further backward at $\beta \approx 150°$. It can be attributed to the ship's chimney that lies in the respective direction seen from the setup (cf. Figure 1).

For low elevations, the distribution is similar to the medium range one, slightly more balanced and with two clear disturbances in main mast and chimney directions, with $\beta \approx 45°$ and $\beta \approx 150°$, respectively. Considering the lowest elevation, the number of disturbances increases. However, they are not as easy to attribute apart from the chimney effect.

It is found that the medium elevation range has the most observations, with a peak of >5000, although it only spans 15°. The lowest elevation range has the least observations, with a peak of <800. The systematic disturbances due to main mast and chimney require masking the data. Observation links on the entire starboard side ($0° < \beta < 180°$) are masked out for further analysis. In general, the systematic disturbances reach values σ_ϕ of up to 0.4 rad, and a relevant signature beyond 0.5 rad is not found.

3.2 Ionospheric Anomaly

For a better understanding of ionospheric effects on σ_ϕ, the ionospheric piercing point (IPP) of each satellite link is computed at the F-layer maximum (assuming a height of 350 km), and the local time at the IPP is determined. Figure 4 shows the respective 2D histogram of σ_ϕ resolved in IPP local time. The previously defined elevation ranges (high, medium, low, and lowest) are distinguished. The distribution over local time differs significantly among the elevation ranges.

In the high elevation range, the least observations occur between 4 h and 12 h, while the peak is at about 23 h. For medium elevations, the least observations are found between 12 h and 20 h, while the peak is at about 7 h. Low and lowest elevations show a more periodic pattern. Especially for low elevations, a period of 4 h is detected. The distribution over local time, in general, has geometrical reasons and is influenced by the ship's heading and the applied masking of starboard observations. The features of distributions seen in Figure 4 are also found if we consider simulations, as shown in Figure 5. The simulated links almost completely agree with the observed links in this central Arctic period. Only at lowest elevations, the observed links are significantly below the simulated links. The simulations are only based on the geometric settings (heading and mask), meaning that these features, for example, the 4 h period at low elevations, have geometric reasons.

The baseline level of σ_ϕ, even after filtering mast and chimney disturbances, is still rather high (0.1 rad and above). For ground-based stations with the same equipment, this level is lower, up to 0.05 rad. A threshold > 0.1 rad can be used to detect scintillation [13]. Here, a threshold > 0.15 rad is required in high- and medium-range observations. Even higher thresholds are needed to find anomalies at lower observations. A significant anomaly, which is related to the geometrical simulations, occurs in the high elevation range at about 10 h. There, σ_ϕ is about 80% above the baseline level (≈0.1 rad). According to climatological studies on GPS phase scintillation [13], this increase of σ_ϕ around noon local time can be attributed to electron density variation in the ionosphere of the cusp region.

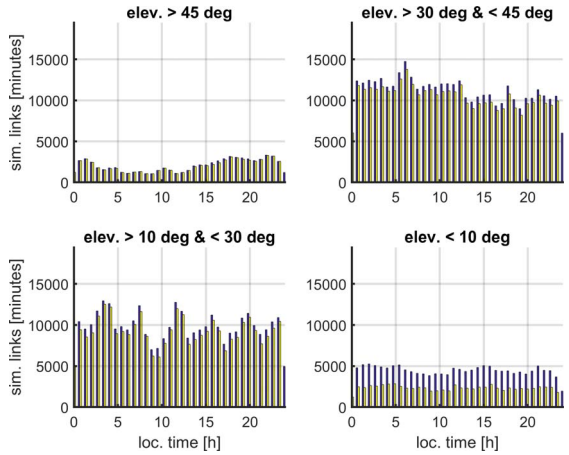

Figure 5. Distribution of simulated and observed links (blue and yellow bars, respectively). Panels with high, medium, low, and lowest elevations are distinguished.

4. Conclusions

The results indicate that ionospheric variations in the Arctic cusp region can be detected using GNSS data from a ship. A masking of relative bearing is required to mitigate the impact of ship-based structures (mast and chimney). The resolved ionosphere-related anomalies of about 0.15 rad to 0.2 rad indicate a moderate level of ionospheric disturbance, as expected in this period of low solar activity. The anomaly around noon local time, indicating particle precipitation in the cusp region, is found at high elevations. An increased level also appears at medium elevations. At a lower elevation, this feature no longer occurs. This limit to higher elevation can be explained by the relation of latitude and elevation for observers in the central Arctic. Only high elevation observations have an IPP in the central Arctic (at high latitudes), where the cusp influence can be found. Analyzing the distribution of σ_ϕ (over relative bearing and local time) is a reasonable starting point to reveal space weather effects. A deeper analysis of phase data for the resolution diffractive or refractive effects is left to future studies. The 1 min integrated scintillation index, considered here, limits the spatial scale resolution. Future studies may concentrate on bitgrabber data for an adapted resolution in a software receiver approach. It is especially promising for kinematic scenarios (e.g., on a ship) when the baseline level of σ_ϕ can be rather high.

5. Acknowledgments

Data used in this manuscript were derived as part of the Multidisciplinary Drifting Observatory for the Study of Arctic Climate (MOSAiC) expedition (tag MOSAiC20192020; project AWI_PS122_0). We are grateful for the support of Lothar Kurz and Simon Plass on preparing and mounting the global navigation satellite system setup. The crew and science team of Polarstern, the Alfred Wegener Institute, and MOSAiC are gratefully acknowledged for running this project. Special thanks to Gunnar Spreen for coordinating the MOSAiC remote sensing group and to the other data contributors: Lars Kaleschke, Robert Ricker, and Aikaterini Tavri who supervised the measurements during the expedition.

6. References

1. Alfred-Wegener-Institut Helmholtz-Zentrum fur Polar- und Meeresforschung, “Polar Research and Supply Vessel POLARSTERN Operated by the Alfred-Wegener-Institute,” *Journal of Large-Scale Research Facilities*, **3**, January 2017, p. A119.
2. U. Nixdorf, K. Dethloff, M. Rex, M. Shupe, A. Sommerfeld, et al., “MOSAiC Extended Acknowledgement,” http://dx.doi.org/10.5281/zenodo.5541624 (Accessed April 2023).
3. J. Wang, Z. Wu, M. Semmling, F. Zus, S. Gerland, et al., “Retrieving Precipitable Water Vapor From Shipborne Multi-GNSS Observations,” *Geophysical Research Letters*, **46**, 9, May 2019, pp. 5000-5008.
4. B. Männel, F. Zus, G. Dick, S. Glaser, M. Semmling, et al., “GNSS-Based Water Vapor Estimation and Validation During the MOSAiC Expedition,” *Atmospheric Measurement Techniques*, **14**, 7, July 2021, pp. 5127-5138.
5. A. M. Semmling, A. Rösel, D. Divine, S. Gerland, G. Stienne, et al., “Sea Ice Concentration Derived From GNSS Reflection Measurements in Fram Strait,” *IEEE Transactions on Geoscience and Remote Sensing*, **57**, 12, 2019, pp. 10350-10361.
6. J. F. Munoz-Martin, A. Perez, A. Camps, S. Ribó, E. Cardellach, et al., “Snow and Ice Thickness Retrievals Using GNSS-R: Preliminary Results of the MOSAiC Experiment,” *Remote Sensing*, **12**, 24, December 2020, p. 4038.
7. A. M. Semmling, J. Wickert, F. Kress, M. M. Hoque, D. V. Divine, et al., “Sea-Ice Permittivity Derived From GNSS Reflection Profiles: Results of the MOSAiC Expedition,” *IEEE Transactions on Geoscience Remote Sensing*, **60**, October 2021, p. 4302416.
8. P. M. Kintner, B. M. Ledvina, and E. R. de Paula, “GPS and Ionospheric Scintillations,” *Space Weather*, **5**, 9, September 2007, p. S09003.
9. M. Kriegel, N. Jakowski, J. Berdermann, H. Sato, and M. W. Mersha, “Scintillation Measurements at Bahir Dar During the High Solar Activity Phase of Solar Cycle 24,” *Annales Geophysicae*, 35, 1, January 2017, pp. 97-106.
10. L. Spogli, L. Alfonsi, G. De Franceschi, V. Romano, M. H. O. Aquino, et al., “Climatology of GPS Ionospheric Scintillations Over High and Mid-Latitude European Regions,” *Ann. Geophys*, **27**, 9, September 2009, pp. 3429-3437.
11. F. Fohlmeister, L. Kurz, M. Kriegel, G. Spreen, and A. Immerz, “Processed 1 Minute Scintillation Measurements From POLARSTERN Deck During the MOSAiC Expedition With POLARSTERN to the Arctic,” https://doi.pangaea.de/10.1594/PANGAEA.956019 (Accessed April 2023).
12. Y. Wang, Q.-H. Zhang, P. T. Jayachandran, J. Moen, Z.-Y. Xing, et al., “Experimental Evidence on the Dependence of the Standard GPS Phase Scintillation Index on the Ionospheric Plasma Drift Around Noon Sector of the Polar Ionosphere,” *Journal of Geophysical Research: Space Physics*, **123**, 3, March 2018, pp. 2370-2378.
13. P. Prikryl, P. T. Jayachandran, R. Chadwick, and T. D. Kelly, “Climatology of GPS Phase Scintillation at Northern High Latitudes for the Period From 2008 to 2013,” *Annales Geophysicae*, **33**, 5, May 2015, pp. 531-545.